

Modal locking between vocal fold and vocal tract oscillations: Simulations in time domain

A. Aalto^{1,4}, T. Murtola^{1,3}, J. Malinen^{1,*}, D. Aalto^{2,5}, M. Vainio²

December 3, 2024

Abstract

It is well known that during voiced speech, the human vocal folds interact with the vocal tract acoustics. The resulting source-filter coupling has been observed using mathematical and physical models as well as in *in vivo* phonation.

We propose a computational time-domain model of the full speech apparatus that, in particular, contains a feedback mechanism from the vocal tract acoustics to the vocal fold oscillations. It is based on numerical solution of ordinary and partial differential equations defined on vocal tract geometries that have been obtained by Magnetic Resonance Imaging. The model is used to simulate rising and falling pitch glides of [a, i] in the fundamental frequency (f_0) interval [180 Hz, 360 Hz]. The interval contains the first formant F_1 of [i] as well as the subformants $F_1/4$ and $F_1/3$ of [a].

The simulations reveal a locking pattern of the f_0 -trajectory at F_1 of [i] in falling and rising glides. The subformants of [a] produce perturbations in the waveforms of glottal signals but no locking. All these observations from the model behaviour are consistent and robust within a wide range of feasible model parameter values and under exclusion of secondary model components. The simulation results suggest that the leading source of discrepancy between the model and true speech biophysics in vowels at frequencies under 4 kHz is due to simplified flow modelling. The characteristics of the simulated locking pattern can be used for developing a high-resolution statistical instrument for detection of the same pattern in experimental material.

Index Terms: Speech modelling, vocal fold model, flow induced vibrations, modal locking.

¹Dept. of Mathematics and Systems Analysis, Aalto University, Finland

²Institute of Behavioural Sciences (SigMe group), University of Helsinki, Finland

³Dept. of Signal Processing and Acoustics, Aalto University, Finland

⁴INRIA, Saclay Ile-de-France Research Center, France

⁵Speech Communication and Disorders, University of Alberta, Canada

* Corresponding author: jarmo.malinen@aalto.fi

1 Introduction

The classical source–filter theory of vowel production is built on the assumption that the source (i.e., the vocal fold vibration) operates independently of the filter (i.e., the vocal tract, henceforth VT) whose resonances modulate the resulting vowel sound [1, 2]. Even though this approach captures a wide range of phenomena in speech production, at least in male speakers, some observations remain unexplained by the source–filter model lacking feedback. The purpose of this article is to deal with some of these observations using computational modelling.

More precisely, simulated rising and falling frequency glides of vowels [a] and [i] over the frequency range [180 Hz, 360 Hz] are considered. Similar glides recorded from eleven female test subjects are treated in the companion article [3]. Such a vowel glide is particularly interesting if its glottal frequency (f_0) range intersects an isolated acoustic resonance of the supra- or subglottal cavity, which we here assume to correspond to the lowest VT formant F_1 . Since F_1 almost always lies high above f_0 in adult male phonation, this situation occurs typically in female subjects and only when they are producing vowels such as [i] with low F_1 . As reported in Section 7, simulations reveal (in addition to other observations) a characteristic locking behaviour of f_0 at the VT acoustic resonance $R_1 \approx F_1$. To check the robustness of the model observations, secondary features of the model are discussed in Section 8, and the role of unmodelled physics is considered in Section 9.

As a matter of fact, this article has two equally important objectives. Firstly, we pursue better understanding of the time-domain dynamics of glottal pulse perturbations near F_1 of [i] and at other acoustic “hot spots” of the VT and the subglottal system within [180 Hz, 360 Hz] that may be reached in speech or singing. Obviously, an acoustic and flow-mechanical model of the speech apparatus is a suitable tool for this purpose. Secondly, we introduce and validate a computational model that meets these requirements. The proposed model has been originally designed to be a glottal pulse source for high-resolution 3D computational acoustics model of the VT which is being developed for medical purposes [4, 5]. There is an emerging application for this model as a development platform of speech signal processing algorithms such as discussed in [6, 7, 8]; however, the model introduced in [9] by Story has been used in [6]. Since perturbations of f_0 near F_1 are a widely researched, yet quite multifaceted phenomenon, it is a good candidate for model validation and benchmarking experiments.

Simulations indicate special kinds of perturbations in vocal folds vibrations near a VT resonance as described in Section 7. The mere existence of such perturbations is hardly surprising considering the wide range of existing literature. Since the seminal work [10] of Ishizaka and Flanagan in 1972, the resonance perturbation problem has been approached from many other directions: experiments on excised larynges mounted on a resonator by Austin and Titze [11], physical models without tissue components with variable subglottal res-

We denote the VT resonances by letters R_1, R_2, \dots to keep them conceptually apart from the formants F_1, F_2, \dots . The resonances are understood here as purely mathematical objects, determined by an acoustic PDE and its boundary conditions that are defined on the VT geometry. Formants refer to respective frequency peaks extracted from natural speech. Of course, we expect to have $R_j \approx F_j$ for $j = 1, 2, \dots$.

onators by Zhang et al. [12] and Lucero et al. [13], and reasoning based on sub- and supraglottal impedances combined with a non-computational flow model by Titze [14]. A two-mass model of vocal folds, coupled with a variable-length resonator tube, was used by Hatzikirou et al. [15], and pitch glides were simulated using a four-mass model to analyse the interactions between vocal register transitions and VT resonances by Tokuda et al. [16]. All these works reveal a consistent picture of the existence of a perturbation pattern, and it has also been detected experimentally by Titze et al. [17] using speech recordings and by Zañartu et al. [18] using simultaneous recordings of laryngeal endoscopy, acoustics, aerodynamics, electroglottography, and acceleration sensors. The latter article also contains a review on related voice bifurcations.

Many earlier models of phonation were based on the Kelly–Lochbaum vocal tract [19] or various transmission line analogues [20, 21, 22]. Contrary to these approaches, the proposed model consists of (ordinary and partial) differential equations, conservation laws, and coupling equations introduced in Sections 2–4. In particular, the curvature of the vocal tract as well as acoustic losses to tissues are explicitly included in the mathematical description. In this modelling paradigm, the temporal and spatial discretisation is conceptually and practically separated from the actual mathematical model of speech. The computational model is simply a numerical solver for the model equations, written in MATLAB environment. The modular design makes it easy to decouple model components for assessing their significance to simulated behaviour. Since the generalised Webster’s equation for the VT acoustics assumes intersectional area functions as its geometric data, VT configurations from Magnetic Resonance Imaging (MRI) can be used without transcription to non-geometric model parameters. Thus, time-dependent VT geometries are easy to implement. Further advantages of speech modelling based on Webster’s equation have been explained in [24, Section 1] where the approach is somewhat similar to one taken here.

The proposed model aims at qualitatively realistic functionality, tunability by a low number of parameters, and tractability of model components, equations, and their relation to biophysics. Similar functionality in higher precision can be obtained using Computational Fluid Dynamics (CFD) with elastic tissue boundaries. In the CFD approach, the aim is to model the speech apparatus as undivided whole [25, 26], but the computational cost is much higher compared to our model or the models proposed in, e.g., [24, 27]. The numerical efficiency is a key issue because some parameter values or their feasible ranges (in particular, for hard-to-get physiological parameters) can only be determined by the trial and error method. This leads to a high number of simulation runs as reported in [28, Chapter 4].

2 Model of the vocal folds

2.1 Anatomy, physiology, and control of phonation

All voiced speech sounds originate from self-sustained quasi-periodic oscillations of the vocal folds where the closure of the aperture — known as the *rima glottidis*

Some economy of modelled features should be maintained to prevent various forms of “overfitting” while explaining the experimental facts. Good modelling practices within mathematical acoustics have been discussed in [23, Chapter 8].

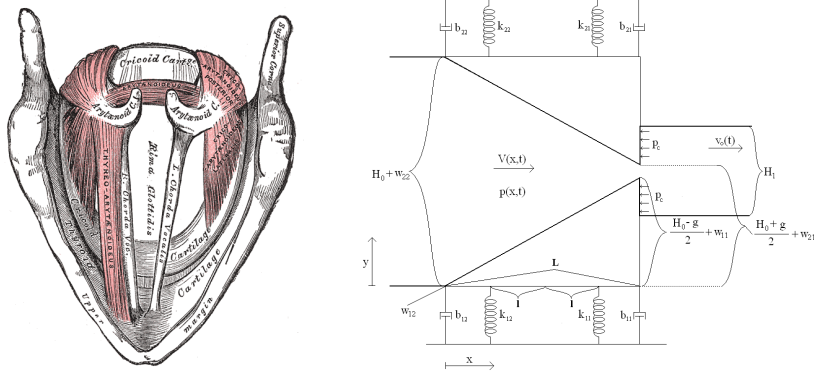


Figure 1: Left: Sketch of the anatomy of the larynx seen from above according to [29, Fig. 960]. Right: The geometry of the glottis model and the symbols used. The trachea (i.e., the channel leading from the lungs to glottis) is to the left in this sketch and the vocal tract is to the right.

— between the two string-like vocal folds cuts off the air flow from lungs. This process is called phonation, and the system comprising the vocal folds and the rima glottidis is known as the glottis. A single period of the glottal flow produced by phonation is known as a glottal pulse.

As shown in Fig. 1 (left panel), each vocal fold consists of a vocal ligament (also known as a vocal cord) together with a medial part of the thyroarytenoid muscle, and the vocalis muscle that (not specified in Fig. 1). Left and right vocal folds are attached to the thyroid cartilage from their anterior ends and to the respective left and right arytenoid cartilages from their posterior ends. In addition, there is the fourth, ring-formed cricoid cartilage whose location is inferior to the thyroid cartilage. The vocal folds and the associated muscles are supported by these cartilages.

There are two muscles attached between each of the arytenoid cartilages and the cricoid cartilage: the posterior and the lateral cricoarytenoid muscles whose mechanical actions are opposite. The vocal folds are adducted by the contraction of the lateral cricoarytenoid muscles during phonation, and conversely, abducted by the posterior cricoarytenoid muscles during, e.g., breathing. This control action is realised by a rotational movement of the arytenoid cartilages in a transversal plane. In addition, there is a fifth (unpaired) muscle — the arytenoid muscle — whose contraction brings the arytenoid cartilages closer to each other, thus reducing the opening of the glottis independently of the lateral cricoarytenoid muscles. These rather complicated control mechanisms regulate the type of phonation in the breathy-pressed scale.

The main mechanism controlling the fundamental frequency f_0 of voiced speech sound is actuated by two cricothyroid muscles (not visible in Fig. 1). The contraction of these muscles leads to a rotation of the thyroid cartilage with respect to the cricoid cartilage. As a result, the thyroid cartilage inclines to the anterior direction, thus stretching the vocal folds. The elongation of the string-like vocal folds leads to increased stress which raises the fundamental frequency f_0 of their longitudinal vibrations. The vertical movement of larynx also rotates cricoid cartilage impacting f_0 . Finally, the phonation and f_0 are

influenced by subglottal pressure through the control of respiratory muscles.

2.2 Glottis model

The anatomic configuration in Fig. 1 (left panel) is idealised as a low-order mass-spring system with aerodynamic surfaces as shown in Fig. 1 (right panel) and discussed in [30, 31, 28]. Such lumped-element models have been used frequently (see, e.g., [32, 33, 34, 35, 36]) since the introduction of the classic two-mass model [10] by Ishizaka and Flanagan in 1972. For recent reviews of the variety of lumped-element and PDE based models and their applications, see [37, 38, 39].

The radically simplified glottis model geometry in Fig. 1 (right panel) corresponds to the coronal section through the center of the vocal folds. Both the fundamental frequency f_0 as well as the phonation type can be chosen by adjusting parameter values, see [28, Section 4]. Register shifts (e.g., from modal register to falsetto) are not in the scope of this model since it would require either modelling the vocal folds as aerodynamically loaded strings or as a high-order mass-spring system that has a string-like “elastic” behavior.

The vocal fold model in Fig. 1 (right panel) consists of two wedge-shaped moving elements that have two degrees of freedom each. The distributed mass of these elements can be reduced into three mass points which are located so that m_{j1} is at $x = L$, m_{j2} at $x = 0$, and m_{j3} at $x = L/2$. Here L denotes the thickness of the modelled vocal fold structures. The elastic support of the vocal ligament is approximated by two springs at points $x = l_1 L = L/2 + l$ and $x = l_2 L = L/2 - l$. The equations of motion for the vocal folds are given by

$$\begin{cases} M_1 \ddot{W}_1(t) + B_1 \dot{W}_1(t) + K_1 W_1(t) = -F(t), \\ M_2 \ddot{W}_2(t) + B_2 \dot{W}_2(t) + K_2 W_2(t) = F(t), \end{cases} \quad t \in \mathbb{R}. \quad (1)$$

where $W_j = [w_{j1} \ w_{j2}]^T$ are the displacements of the right and left endpoints of the j^{th} fold, $j = 1, 2$, as shown in Fig. 1 (right panel). The respective mass, damping, and stiffness matrices M_j , B_j , and K_j in (1) are

$$M_j = \begin{bmatrix} m_{j1} + \frac{m_{j3}}{4} & \frac{m_{j3}}{4} \\ \frac{m_{j3}}{4} & m_{j2} + \frac{m_{j3}}{4} \end{bmatrix}, \quad B_j = \begin{bmatrix} b_{j1} & 0 \\ 0 & b_{j2} \end{bmatrix}, \quad (2)$$

$$\text{and} \quad K_j = \begin{bmatrix} l_1^2 k_{j1} + l_2^2 k_{j2} & l_1 l_2 (k_{j1} + k_{j2}) \\ l_1 l_2 (k_{j1} + k_{j2}) & l_2^2 k_{j1} + l_1^2 k_{j2} \end{bmatrix}.$$

The entries of these matrices have been computed by means of Lagrangian mechanics. The damping matrices B_j are diagonal since the dampers are located at the endpoints of the vocal folds. The model supports asymmetric vocal fold vibrations but for this work symmetric vocal fold parameters are used (i.e. $M = M_j$, $K = K_j$, and $B = B_j$, $j = 1, 2$).

The glottal openings at the two ends of the vocal folds, denoted by ΔW_i , $i = 1, 2$, are related to Eqs. (1) through

$$\begin{bmatrix} \Delta W_1 \\ \Delta W_2 \end{bmatrix} = W_2 - W_1 + \begin{bmatrix} g \\ H_0 \end{bmatrix}, \quad (3)$$

where the rest gap parameters g and H_0 are as in Fig. 1 (right panel). In human anatomy, the parameter g is related to the position and orientation of the

arytenoid cartilages. During the glottal open phase (i.e., when $\Delta W_1(t) > 0$ at the narrow end of the vocal folds), the load terms in Eq. (1) are given by $F = [F_{A,1} \ F_{A,2}]^T$ as introduced below in Eq. (7) in terms of the aerodynamic forces from the glottal flow. During the glottal closed phase (i.e., when $\Delta W_1(t) < 0$), there are no aerodynamic forces apart from the joint acoustic counter pressure, denoted by p_c in Eq. (12), from the VT and subglottal cavities as properly introduced in Section 4 below. Instead, the acoustic counter pressure is accompanied by a nonlinear spring force with parameter k_H , accounting for the elastic collision of the vocal folds and given by

$$F = \begin{bmatrix} k_H |\Delta W_1|^{3/2} - \frac{H_0 - H_1/2}{2L} \frac{H_1}{2} h \cdot p_c \\ \frac{H_0 - H_1/2}{2L} \frac{H_1}{2} h \cdot p_c \end{bmatrix}. \quad (4)$$

This is related to the Hertz impact model that has been used similarly in [40, 32].

As is typical in related biomechanical modelling [16, 32, 41], the lumped parameters of the mass-spring system (1)–(2) are in some correspondence to true the masses, material parameters, and geometric characteristics of the sound producing tissues. More precisely, matrices M correspond to the vibrating masses of the vocal folds, including the vocal ligaments together with their covering mucous layers and (at least, partly) the supporting vocalis muscles. The elements of the matrices K , are best understood as linear approximations of $k(s) = f/s$ where $f = f(s)$ is the contact force required for deflection s at the center of the string-like vocal ligament in Fig. 1 (left panel). It should be emphasised that the exact numerical correspondence of tissue parameters to lumped model parameters M and K is intractable (and for most practical purposes even irrelevant), and their values in computer simulations must be tuned using measurement data of f_0 and the measured form of the glottal pulse [42, 28].

3 Glottal flow and the aerodynamic force

An incompressible one-dimensional flow through the glottal opening with velocity v_o is described by

$$\dot{v}_o(t) = \frac{1}{C_{iner} h H_1} (p_{sub} - R_g(t) v_o(t)), \quad (5)$$

where p_{sub} is the subglottal static (lung) pressure above ambient pressure, C_{iner} regulates flow inertia, h is the width of the rectangular flow channel, and $R_g(t)$ represents the total pressure loss in the glottis. In fact, Eq. (5) is related to Newton's second law for the air column in motion. The total pressure loss consists of two components, namely

$$\begin{aligned} R_g(t) &= R_v(t) + R_t(t) \quad \text{where} \\ R_v(t) &= \frac{12\mu H_1 L_g}{\Delta W_1(t)^3} \quad \text{and} \quad R_t(t) = k_g \frac{\rho H_1^2 v_o(t)}{2\Delta W_1(t)^2}. \end{aligned} \quad (6)$$

The first term $R_v(t)$ represents the viscous pressure loss, and it is motivated by the Hagen–Poiseuille law in a narrow aperture. It approximates the pressure loss in the glottis using a rectangular tube of width h , height ΔW_1 , and length L_g . The parameter μ is the kinematic viscosity of air. The second term $R_t(t)$ takes

into account the pressure loss due to turbulence, and its form is motivated by the experimental work in [43, Eq. (4) on p. 628]. The coefficient k_g represents the difference between turbulent energy loss at the glottal inlet and pressure recovery at the outlet. This coefficient depends not only on the glottal geometry but also on the glottal opening, subglottal pressure, and flow through the glottis [44].

In the glottis, the flow velocity $V(x, t)$ is assumed to satisfy the mass conservation law $H(x, t)V(x, t) = H_1 v_o(t)$ for incompressible flow where $H(x, t)$ is the height of the flow channel inside the glottis. In the model geometry of Fig. 1 (right panel), we have

$$H(x, t) = \Delta W_2(t) + \frac{x}{L}(\Delta W_1(t) - \Delta W_2(t)), \quad x \in [0, L].$$

Now, the pressure $p = p(x, t)$ in the glottis is given in terms of v_0 from Eq. (5) by these two equations and the Bernoulli law $p(x, t) + \frac{1}{2}\rho V(x, t)^2 = p_{sub}$ for static flow.

Since each vocal fold has two degrees of freedom, the pressure p in the glottis and the VT/SGT counter pressure p_c can be reduced to an aerodynamic force pair $[F_{A,1} \ F_{A,2}]^T$ where $F_{A,1}$ affects at the right (i.e., the superior) end of the glottis ($x = L$) and $F_{A,2}$ the left (i.e., the inferior) end ($x = 0$) in Fig. 1 (right panel). This reduction can be carried out by using the total force and moment balance equations

$$F_{A,1} + F_{A,2} = h \int_0^L (p(x, t) - p_{sub}) dx$$

and

$$L \cdot F_{A,1} = h \int_0^L x(p(x, t) - p_{sub}) dx - p_c \cdot h \frac{H_1}{2} \frac{H_0 - H_1/2}{2}.$$

The moment is evaluated with respect to point $(x, y) = (0, 0)$ for the lower fold and $(x, y) = (0, H_0)$ for the upper fold in Fig. 1 (right panel). Evaluation of these integrals yields

$$\begin{cases} F_{A,1} = \frac{1}{2}\rho v_o^2 h L \left(-\frac{H_1^2}{\Delta W_1(\Delta W_2 - \Delta W_1)} + \frac{H_1^2}{(\Delta W_1 - \Delta W_2)^2} \ln \left(\frac{\Delta W_2}{\Delta W_1} \right) \right) - \frac{H_1(H_0 - H_1/2)}{4L} h p_c, \\ F_{A,2} = \frac{1}{2}\rho v_o^2 h L \left(\frac{H_1^2}{\Delta W_2(\Delta W_2 - \Delta W_1)} - \frac{H_1^2}{(\Delta W_1 - \Delta W_2)^2} \ln \left(\frac{\Delta W_2}{\Delta W_1} \right) \right) + \frac{H_1(H_0 - H_1/2)}{4L} h p_c. \end{cases} \quad (7)$$

4 Vocal tract and subglottal acoustics

4.1 Modelling VT acoustics by Webster's equation

A generalised version of Webster's horn model resonator is used as acoustic loads to represent both the VT and the SGT. It is given by

$$\frac{1}{c^2 \Sigma(s)^2} \frac{\partial^2 \psi}{\partial t^2} + \frac{2\pi\alpha W(s)}{A(s)} \frac{\partial \psi}{\partial t} - \frac{1}{A(s)} \frac{\partial}{\partial s} \left(A(s) \frac{\partial \psi}{\partial s} \right) = 0, \quad (8)$$

where c denotes the speed of sound, the parameter $\alpha \geq 0$ regulates the energy dissipation through air-tissue interface, and the solution $\psi = \psi(s, t)$ is the

velocity potential of the acoustic field. Then the sound pressure is given by $p = \rho\psi_t$ where ρ denotes the density of air. The generalised Webster's model for acoustic waveguides has been derived from the wave equation in a tubular domain in [45], its solvability and energy notions have been treated in [46], and the approximation properties in [47].

The generalised Webster's equation (8) is applicable if the VT is approximated as a curved tube of varying cross-sectional area and length L_{VT} . The centreline $\gamma : [0, L_{VT}] \rightarrow \mathbb{R}^3$ of the tube is parametrised using distance $s \in [0, L_{VT}]$ from the superior end of the glottis, and it is assumed to be a smooth planar curve. At every s , the cross-sectional area of the tube perpendicular to the centreline is given by the area function $A(s)$, and the (hydrodynamic) radius of the tube, denoted by $R(s) > 0$, is defined by $A(s) = \pi R(s)^2$. The curvature of the tube is defined as $\kappa(s) := \|\gamma''(s)\|$, and the curvature ratio as $\eta(s) := R(s)\kappa(s)$. Since the tube does not fold on to itself, we have always $\eta(s) < 1$, and clearly $\eta \equiv 0$ if the tube is straight.

We are now ready to describe the rest of the parameters appearing in Eq. (8): They are the stretching factor $W(s)$ and the sound speed correction factor $\Sigma(s)$, defined by

$$\begin{aligned} W(s) &:= R(s)\sqrt{R'(s)^2 + (\eta(s) - 1)^2}, \\ \Sigma(s) &:= (1 + \frac{1}{4}\eta^2(s))^{-1/2}. \end{aligned} \quad (9)$$

In the context of VT, we use the following boundary conditions for Eq. (8):

$$\begin{cases} \frac{\partial\psi}{\partial t}(L_{VT}, t) + \theta c \frac{\partial\psi}{\partial s}(L_{VT}, t) &= 0, \\ \frac{\partial\psi}{\partial s}(0, t) &= -c_1 v_0(t). \end{cases} \quad (10)$$

The first boundary condition is imposed at the mouth opening, and the parameter $\theta \geq 0$ is the normalised acoustic resistance due to exterior space [48, Chapter 7]. The latter boundary condition in Eq. (10) couples the resonator to the glottal flow given by Eq. (5). The scaling parameter $c_1 = H_1 h/A(0)$ extends the assumption of incompressibility from the control area just right to the glottis in Fig. 1 (right panel) to the VT area slice nearest to the glottis.

4.2 Subglottal tract acoustics

Anatomically, the SGT consists of the airways below the larynx: trachea, bronchi, bronchioles, alveolar ducts, alveolar sacs, and alveoli. This system has been modelled either as a tree-like structure [27] or, more simply, as an acoustic horn whose area increases towards the lungs [49, 34]. We take the latter approach and denote the cross-sectional area and the horn radius by $A_s(s)$ and $R_s(s)$, respectively, where $s \in [0, L_{SGT}]$ and L_{SGT} is the nominal length of the SGT.

Since the subglottal horn is assumed to be straight, i.e. $\eta \equiv 0$, we have $\Sigma \equiv 1$ and $W_s(s) = R_s(s)\sqrt{R'_s(s)^2 + 1}$. Then Eqs. (8)–(10) translate to

$$\begin{cases} \frac{1}{c^2} \frac{\partial^2 \tilde{\psi}}{\partial t^2} + \frac{2\pi\alpha W_s(s)}{A_s(s)} \frac{\partial \tilde{\psi}}{\partial t} - \frac{1}{A_s(s)} \frac{\partial}{\partial s} \left(A_s(s) \frac{\partial \tilde{\psi}}{\partial s} \right) &= 0, \\ \frac{\partial \tilde{\psi}}{\partial t}(L_{SGT}, t) + \theta_s c \frac{\partial \tilde{\psi}}{\partial s}(L_{SGT}, t) &= 0, \\ \frac{\partial \tilde{\psi}}{\partial s}(0, t) &= c_2 v_0(t), \end{cases} \quad (11)$$

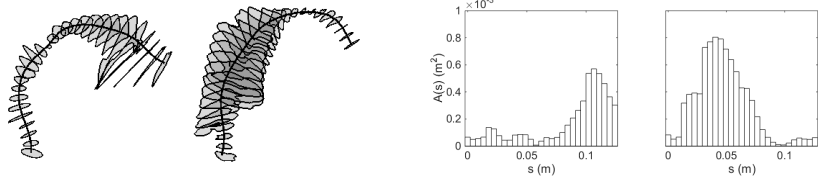


Figure 2: Left: The VT intersections extracted from the test subject during phonation of [q] and [i]. Right: The resulting area functions for Eq. (8), represented as a function of distance from the glottis.

where the solution $\tilde{\psi}$ is the velocity potential for the SGT acoustics. Again, the parameter $\theta_s \geq 0$ is the normalised acoustic resistance at the lung end of the horn, and we now use the scaling parameter value $c_2 = H_1 h / A_s(0)$.

4.3 The acoustic counter pressure

The final part of the vowel model produces the feedback coupling from VT/SGT acoustics back to glottal oscillations. This coupling is realised by the acoustic counter pressure $p_c = p_c(t)$ that already makes appearance in Eqs. (4) and (7) above. The counter pressure is the resultant of sub- and supraglottal pressure components, and it is given in terms of velocity potentials from Eqs. (8) and (11) by

$$p_c(t) = Q_{pc} \rho \left(\psi_t(0, t) - c_3 \tilde{\psi}_t(0, t) \right). \quad (12)$$

The tuning parameter $Q_{pc} \in [0, 1]$ enables scaling the magnitude of the feedback from the VT and SGT resonators to the vocal folds. The parameter Q_{pc} is necessary because it is difficult to estimate from anatomic data the area on which the counter pressure p_c acts. In simulations, excessive acoustic load forces lead to non-stationary, even chaotic vibrations of the vocal folds.

The second parameter $c_3 \geq 0$ in Eq. (12) accounts for the differences in the areas and moment arms for the supra- and subglottal pressures that load the equations of motion Eqs. (1) for vocal folds. Based on the idealised vocal folds geometry in Fig. 1, we obtain an overly high nominal value $c_3 = 8.6$. In the simulations of this article, we use Q_{pc} as a tuning parameter to obtain the desired glottal pulse waveform, and the value of c_3 is kept fixed (one could say, arbitrarily) at $c_3 = 1$ (if the subglottal resonator is coupled) or $c_3 = 0$ (if the subglottal acoustics is ignored). If it is necessary for producing a realistic balance between supra- and subglottal feedbacks, the value of c_3 can be increased without losing stable phonation up to $Q_{pc} c_3 \approx 0.6$.

5 Anatomic data and model parameters

5.1 Area functions for VT and SGT

Solving Webster's equation requires that the VT is represented with an area function and a centreline, from which curvature information can be computed. Two different VT geometries corresponding to vowels from a healthy 26 years

old female are used: A prolonged [a] produced at fundamental frequency $f_0 = 168$ Hz and similarly produced [i] at $f_0 = 210$ Hz. These geometries have been obtained by Magnetic Resonance Imaging (MRI) using the experimental setting that has been described in [4, 5]. The extraction of the computational geometry from raw MRI data has been carried out by the custom software described in [50, 51]. The VT geometries and the area functions are shown in Fig. 2, and related VT geometry dependent parameter values are given in Table 1.

The piston model in [48, Chapter 7] gives the expression $\theta = 2\pi A(L_{VT})/\ell^2$ for the normalised acoustic resistance in Eq. (10) where we use the nominal wavelength $\ell = 171.5$ mm. The corresponding values for $\theta[a]$, $\theta[i]$ together with the resonances $R_j[a]$, $R_j[i]$ for $j = 1, 2$ are given in Table 1.

Table 1: Physical and physiological parameters dependent on the VT geometry.

Parameter	[a]	[i]
normalised acoustic resistance at mouth, θ	0.042	0.009
inertia parameter, C_{iner}	2370 kg/m ⁴	2570 kg/m ⁴
length of VT, L_{VT}	0.124 m	0.126 m
1st VT resonance, R_1 , from Eqs. (8)–(10)	807 Hz	219 Hz
2nd VT resonance, R_2 , from Eqs. (8)–(10)	2232 Hz	2980 Hz

The MRI data that is used for the VT does not cover all of the SGT. For this reason, an exponential horn is used as the subglottal area function for Eq. (11)

$$A_s(s) = A_s(0)e^{\epsilon s} \quad \text{where} \quad \epsilon = \frac{1}{L_{SGT}} \ln \left(\frac{A_s(L_{SGT})}{A_s(0)} \right) \quad (13)$$

following [49]. The values for $A_s(0) = 2$ cm² and $A_s(L_{SGT}) = 10$ cm² are taken from [49, Fig. 1]. The horn length L_{SGT} is tuned so that the lowest subglottal resonance is $\tilde{R}_1 = 500$ Hz which results in the second lowest resonance at $\tilde{R}_2 = 1230$ Hz. This is, indeed, a reasonable value for \tilde{R}_1 based on [11, Table 1]; see also [52, 53, 40] and [27, Fig. 1a].

5.2 Static parameter values

Table 2 lists the numerical values of physiological and physical constants used in all simulations. Based on the acoustic reflection and transmission coefficients at the air/tissue interface, the value of the energy loss coefficient in Eqs. (8) and (11) is taken as

$$\alpha = \frac{\rho}{\rho_h c_h} = 7.6 \cdot 10^{-7} \frac{\text{s}}{\text{m}}. \quad (14)$$

The SGT lung termination resistance in Eq. (11) is given the value $\theta_s = 1$ which corresponds to an absorbing boundary condition.

All the model parameter values introduced so far are assumed to be equally valid for both female and male phonation, except for vocal fold length h . As we are treating female phonation in this article, it remains to describe the parameter values for Eqs. (1) where the differences between female and male phonation

In fact, she is one of test subjects in the experimental companion article [3].

are most significant. Horáček et al. provide parameter values for M and K for in male phonation [41, 32] but similar data for female subjects cannot be found in literature. Instead, the masses in M are calculated by combining the vocal fold shape function used by Horáček et al. [32] with female vocal fold length reported by Titze [54]. A first estimate for the spring coefficients in K is calculated by assuming that the first eigenfrequency of the vocal folds matches the starting frequency for the simulations. The spring coefficients are then adjusted until simulations produce the desired starting fundamental frequency for the f_0 -glides, giving the constant K^0 for Eqs. (15)–(16). For details of these rather long calculations, see [30, 28].

Table 2: Physical and physiological constants.

Parameter	Symbol	Value
speed of sound in air	c	343 m/s
density of air	ρ	1.2 kg/m ³
kinematic viscosity of air	μ	18.27 μ N s/m ²
vocal fold tissue density	ρ_h	1020 kg/m ³
VT loss coefficient	α	7.6 · 10 ⁻⁷ s/m
spring constant in contact (from [32])	k_H	730 N/m
glottal gap at rest	g	0.3 mm
vocal fold length (from [54])	h	10 mm
vocal fold thickness (from [32])	L	6.8 mm
vocal fold spring location parameter (from [30])	l	0.35L
control area height below glottis	H_0	11.3 mm
control area height above glottis	H_1	1 mm
equivalent gap length for viscous loss in glottis	L_g	1.5 mm
SGT length	L_{SGT}	220 mm
normalised acoustic resistance at lungs	θ_s	1
glottal entrance/exit coefficient	k_g	0.044
subglottal (lung) pressure over the ambient	p_{sub}^0	600 Pa

Let us conclude with a sanity check on the parameter magnitudes for Eq. (1) describing the vocal folds. The total vibrating mass for female phonation is $m_1 + m_2 + m_3 = 0.27$ g and the total spring coefficients are $k_1 + k_2 = 321$ N/m. These nominal values yield $f_0 \approx 180$ Hz for female phonation. If the characteristic thickness of the vocal folds is assumed to be about 5 mm, these parameters yield a magnitude estimate for the elastic modulus of the vocal folds by $E \approx \frac{k_1+k_2}{Lh} \cdot 5 \cdot 10^{-3}$ m ≈ 23.6 kPa. This should be compared to [55, Fig. 7] where estimates are given for the elastic modulus of *ex vivo* male vocal folds where values between 2.0 kPa and 7.5 kPa are proposed for different parts of the vocal fold tissue.

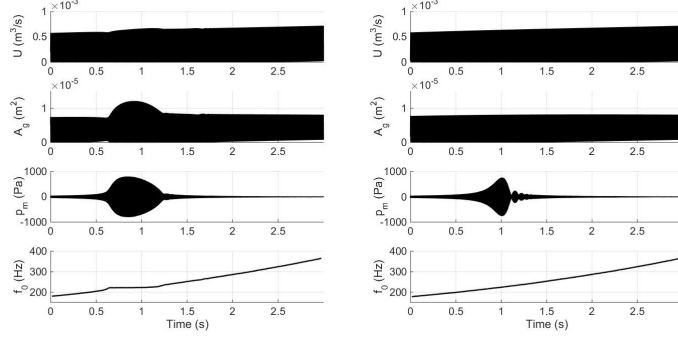


Figure 3: Left: Volume flow (U), glottal area (A_g), sound pressure at lips (p_m), and fundamental frequency (f_0) for a glide for the vowel [i] with $Q_{pc} = 0.1$ and $\beta = 0.046 \text{ kg/s}$. Right: The same glide without VT feedback ($Q_{pc} = 0$). The fundamental frequency has been extracted from the volume flow signal.

6 Computational aspects

6.1 Parameter control for obtaining vowel glides

The f_0 -glide is simulated by controlling two parameter values dynamically. First, the matrix K is scaled while keeping the matrix M constant. This approach is based on the assumption that the vibrating mass of vocal folds is not significantly reduced when the speaker's pitch increases; a reasonable assumption as far as register changes are excluded. The authors would like to remark that the relative magnitudes of M and K essentially determine the resonance frequencies of model (1). However, attention must be paid to their absolute magnitudes using, e.g., dimensional analysis since otherwise the load terms $\pm F(t)$ in Eq. (1) (containing the aerodynamic forces, contact force between the vocal folds during the glottal closed phase, and the counter pressure from the VT/SGT) would scale in an unrealistic manner.

The subglottal pressure, p_{sub} , is the second parameter used to control the glide production. The dependence of the fundamental frequency on p_{sub} has been observed in simulations [10, 56] as well as in humans [57] and excised canine larynges [58]. The impact of p_{sub} on f_0 is, however, secondary in these glides (less than 10 %). Instead, p_{sub} is scaled in order to maintain phonation as the stiffness of the vocal folds changes.

The parameters are scaled exponentially with time

$$K(t) = 2^{2t/T} K^0, \quad p_{sub}(t) = 2^{t/T} p_{sub}^0 \quad (15)$$

for rising glides, and

$$K(t) = 2^{2-2t/T} K^0, \quad p_{sub}(t) = 2^{1-t/T} p_{sub}^0 \quad (16)$$

for falling glides. The duration of the glide is $T = 3 \text{ s}$, and t is the time from the beginning of the glide. Other starting conditions (particularly, vocal fold displacements and velocities, and pressure and velocity distributions in the resonators) are taken from stabilised simulations. These parameters produce glides

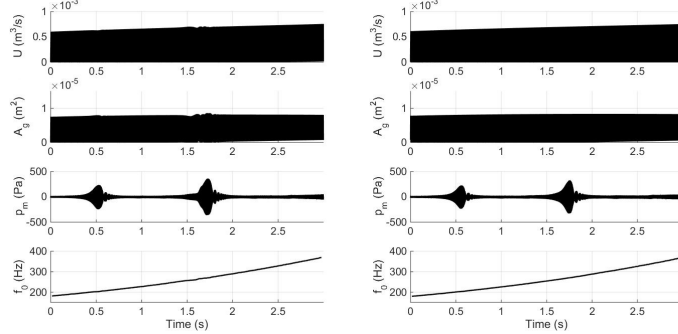


Figure 4: Left: Volume flow (U), glottal area (A_g), sound pressure at lips (p_m), and fundamental frequency (f_0) for a glide for the vowel [a] with $Q_{pc} = 0.2$ and $\beta = 0.046 \text{ kg/s}$. Right: The same glide without VT feedback ($Q_{pc} = 0$).

with f_0 approximately in the range [180 Hz, 360 Hz], although the exact range depends on the VT geometry and vocal fold damping as well.

The damping parameters b_i for $i = 1, 2$, in Eq. (2) play an important but problematic role in glottis models. If there is too much damping (while keeping all other model parameters fixed), sustained oscillations do not occur. Conversely, too low damping will cause instability in simulated vocal fold oscillations. The magnitude of physically realistic damping in vibrating tissues is not available, and the present model could possibly fail to give a quasi-stationary glottis signal even if realistic experimental damping values were used. With some parameter settings, the model even produces quasi-stationary signal at several damping levels. For simplicity, we set $b_i = \beta > 0$ for $i = 1, 2$, and use golden section search to find at least one value of vocal fold loss β that results in stable, sustained oscillation. The damping remains always so small that its lowering effect on the resonances of the mass-spring system (1) is negligible.

6.2 Numerical realisation

The model equations are solved numerically using MATLAB software and custom-made code. The vocal fold equations of motion (1) are solved by the fourth order Runge–Kutta time discretisation scheme. The flow equation (5) is solved by the backward Euler method. The VT is discretised by the FEM using piecewise linear elements ($N = 28$) and the physical energy norm of Webster’s equation. Energy preserving Crank–Nicolson time discretisation (i.e., Tustin’s method [59]) is used. The time step is almost always $10 \mu\text{s}$ which is small enough to keep the frequency warping in Tustin’s method under one semitone for frequencies under 13kHz. Reduced time step, however, is used near glottal closure. This is due to the discontinuity in the aerodynamic force in Eq. (7) at the closure which requires numerical treatment by interpolation and time step reduction as explained in [30, Section 2.4.1].

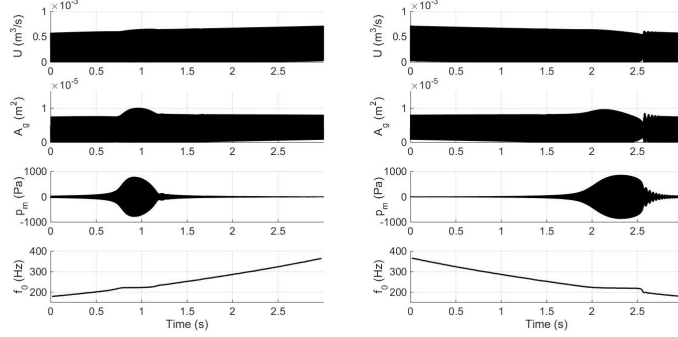


Figure 5: Left: Volume flow (U), glottal area (A_g), sound pressure at lips (p_m), and fundamental frequency (f_0) for an rising glide for the vowel [i] with $Q_{pc} = 0.05$ and $\beta = 0.046 \text{ kg/s}$. Right: The falling glide using the same parameter settings.

7 Simulation results

The results of glide simulations for vowels [a, i] are shown in Figs. 3–4. The fundamental frequency f_0 trajectory has been extracted from the glottal volume flow (i.e., U) signal in all figures.

The simulations indicate a consistent locking pattern at $R_1[i]$ in f_0 trajectories that vanishes if the VT feedback is decoupled by setting $Q_{pc} = 0$. The locking pattern in rising glides follows the representation given in Fig. 6 (right panel): sudden jump upwards to R_1 , a locking to a plateau level, and a smooth release. Such locking behaviour is not observed for glides of [a] where $R_1[a]$ is not inside the simulated frequency range [180 Hz, 360 Hz]. The subresonances $R_1[a]/4 = 201 \text{ Hz}$ and $R_1[a]/3 = 269 \text{ Hz}$ are within the frequency range, and the corresponding events are visible in the sound pressure signal at the lips; see Fig. 4. They do not, however, cause noticeable changes in the f_0 trajectory of the glottal flow. The effect of the loss parameter β on locking pattern has been shown in Fig. 6 (left panel).

Keeping Q_{pc} and other model parameters the same, a falling f_0 glide shows a more pronounced or longer locking at R_1 compared to rising glides; see Fig. 5. In falling glides, there also tend to be "ripples" in f_0 , glottal flow, and glottal area right after the jump downward. Such ripples cannot be observed in rising glides. Using relatively high values of VT feedback parameter Q_{pc} , rising glides will exhibit a sharp corner or an overshoot at the beginning of the plateau which is not observed in falling glides.

Finally, the effect of extreme values of model parameters β and Q_{pc} on the glide simulations at $R_1[i]$ is considered. These observations are qualitatively described in Fig. 6 (middle and right panels). In the right panel, the medium values for β refer to the interval [0.01, 0.05] and for Q_{pc} to the interval [0.05, 0.25]. These intervals can thus be regarded as feasible parameter ranges for vowel glide simulations of [i].

Referring to Fig. 6 (right panel), the full frequency range [180 Hz, 360 Hz] for f_0 can be obtained with modal locking as shown in Fig. 3 if medium Q_{pc} and low-to-medium β are used. Higher Q_{pc} with medium β reduces the simulated f_0

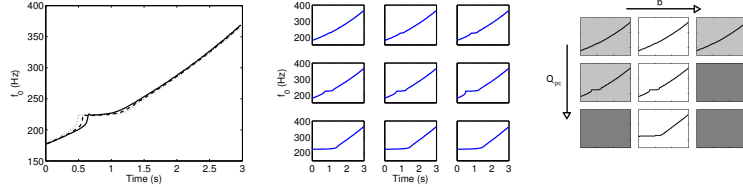


Figure 6: Left: f_0 trajectories for [i] with different values of β and fixed $Q_{pc} = 0.25$. Solid line $\beta = 0.013 \text{ kg/s}$, dashed line $\beta = 0.023 \text{ kg/s}$, and dotted line $\beta = 0.034 \text{ kg/s}$. Middle: f_0 trajectories for [i] with different values of Q_{pc} with $\beta \in [0.03 \text{ kg/s}, 0.05 \text{ kg/s}]$. Values of Q_{pc} from left to right in top row: 0.01, 0.025, and 0.05; middle row: 0.075, 0.1, and 0.25; bottom row: 0.5, 0.75, and 1. Right: f_0 trajectories for [i] qualitatively as Q_{pc} and β increase in the direction of the arrow. Light gray background indicates that few Q_{pc} - β -combinations produce stable simulations; dark gray that no combinations producing stable glides were found.

range to above 220 Hz which is the value of $R_1[i]$; see Fig. 6 (middle panel, three bottom pictures). This glide starting frequency cannot be lowered by changing K , and it appears to represent very strong modal locking at the onset of the vowel glide simulation.

The stability of glide simulations (understood as slowly changing amplitude envelope of glottal volume flow U) becomes a serious issue at low and high values of β . We have tuned the subglottal pressure p_{sub} in glide simulations as given in Eqs. (15)–(16). If we produce the glides with constant p_{sub} , the range of parameter β , giving stable phonation, shifts down a little. Moreover, the range of f_0 shrinks to about [180 Hz, 330 Hz] but the qualitative behaviour of glides and modal locking events remains very similar.

8 Sensitivity and robustness

Parameter tuning of the vowel model is tricky business as can be seen from model parameter optimisation experiments described in [28, Chapter 4]. By exaggerating some of the parameter values, it is possible to make vowel glide simulations over $R_1[i]$ behave in a way that can be excluded by experiments or observations from natural speech.

In phonetically relevant simulations, various tuning parameters must be kept in values that are not only physically reasonable but also do not produce obviously counterfactual predictions. When such a realistic operating point has been found, it remains to make sure that the simulations give consistent and robust results near it. In doing so, we also check which parts of the full model are truly significant for the model behaviour reported in Section 7.

8.1 Acoustics of the vocal tract by Webster's equation

The constant α in Eqs. (8) and (11) regulates the boundary dissipation at the air/tissue interface. As shown in [45, Section 3], it appears in the corresponding dissipating boundary condition $\alpha\phi_t + \bar{\nu} \cdot \nabla \phi = 0$ for the wave equation $\phi_{tt} = c^2 \Delta \phi$ where ϕ is the 3D acoustic velocity potential and $\bar{\nu}$ denotes the exterior normal

of the VT/air boundary. The qualitative effect of physically realistic tissue losses to vowel glide simulations was observed to be insignificant; see also [24, Section 5]. However, these losses move slightly the VT resonance positions computed from Eqs. (8).

On the other hand, the VT resonances are quite sensitive to the normalised acoustic resistance θ in Eq. (10). This parameter regulates the energy loss through mouth to the external acoustic space, and its extreme values 0 and ∞ correspond to open and closed ends for idealised acoustic waveguides, respectively. Again, physically realistic variation in θ does not change the qualitative behaviour of vowel glides near $R_1[i]$ as reported in Section 7.

The role of the VT curvature in Eq. (8) is more involved. As can be seen from Eq. (9), the curvature results in a second order correction in the curvature ratio η to the speed of sound c in Eq. (8). In waveguides of significant intersectional diameter compared to wavelengths of interest, the contribution of η in Eq. (9) appears to be secondary to a larger error source that is related to curvature as well. This is caused by the fact that a longitudinal acoustic wavefront does not propagate in the direction of the geometric centreline of a curved waveguide even if the waveguide were of circular intersection with constant diameter. The wavefront has a tendency to “cut the corners” in a frequency and geometry dependent manner, and we do not have a mathematically satisfying description of the “acoustically correct” centreline that would deal with this phenomenon optimally in the context of Webster’s equation. Extraction of the area function $A(\cdot)$ in Eq. (8) from MR images, however, requires some notion of a centreline, and using a different centreline would lead to slightly different version of $A(\cdot)$. This would somewhat change, e.g., the resonance frequencies of Eq. (8) but not the mathematical structure of the model nor the results of vowel glide simulations reported in Section 7. Hence, we simply use the area functions and centrelines obtained from 3D MR images by the custom code described in [50], using its nominal settings.

It remains to consider the non-longitudinal resonances of the VT. By its construction, the generalised Webster’s equation does not take into account at all the transversal acoustic dynamics of the VT. It is known from numerical 3D Helmholtz resonance experiments on several dozens of VT geometries that lowest non-longitudinal resonances of the human VT tract are at approximately 4 kHz corresponding to $\lambda/2 \approx 4$ cm; see, e.g., [4, Section 5], [60]. Anatomically, such length may appear between opposing valleculae, piriform fossae, or even across the mouth cavity in some VT vowel configurations. However, the upper limit of 4 kHz for Webster’s equation is adequate for the computation of the acoustic counter pressure p_c in Eq. (12) for several octaves lower fundamental frequencies $f_0 \in [180 \text{ Hz}, 360 \text{ Hz}]$ that are used in vowel glide simulations.

8.2 Subglottal acoustics

To large extent, what was stated above about the modelling error of the VT acoustics applies to the SGT acoustics as well. We complement this treatment

It should be pointed out that Eqs. (8)–(9) with nonvanishing η is the “right” generalisation of Webster’s horn model, corresponding to the wave equation in curved acoustic waveguides. This approach results in the approximation error analysis given in [47]. Somewhat paradoxically, a similar error analysis for the simpler model Eqs. (8)–(9) with $\eta \equiv 0$ would require more complicated error estimation.

by considering how and to what extent subglottal acoustics plays a role in the vowel glide simulations of Section 7.

Firstly, significant ringing takes place in the subglottal space. This has been verified by *in vivo* measurements [52, 53, 61, 12], using physical models [11, 62], and by mathematically modelling the subglottal acoustics [27] based on anatomic data of trachea and the progressively subdividing system of bronchi and the alveoles [63, 64]. During the open phase, the inertia of the air column from bronchi up to mouth opening is taken into account by C_{iner} in Eq. (5). At closure, the flow velocity v_o drops to zero, and a rarefaction pulse is formed above the vocal folds due to air column inertia in the VT, and this is part of the acoustics modelled by Eq. (8). Similarly, a compression pulse is formed below the vocal folds, known as the “water hammer” in [65]. The subglottal resonator Eq. (11) is mainly excited by the water hammer. Both of these pulses can be seen in the supra- and subglottal pressure signals p_{sp} and p_{sb} in Fig. 7.

The water hammer is the most important component of subglottal ringing, accompanied by its first echo that arrives back to vocal folds after approximately 2 ms delay. The delay corresponds to the lowest subglottal formant between 500 Hz and 600 Hz as reported in [53, 27]. The first echo returns during the glottal closure at least if $f_0 < 150$ Hz and the open quotient (OQ) of the pulse does not exceed 50 %; see [52, Fig. 4] for measurements and [27, Fig. 12] for simulations. The echoes of the water hammer pulse can be clearly seen in Fig. 7 as well but now the first echo returns after the glottis has opened again due to higher values of f_0 and OQ in these simulations.

The observations from simulations indicate that the subglottal acoustics has an observable effect on glottal pulse waveform. The subglottal effect will get more pronounced when $f_0 \rightarrow \tilde{R}_1 = 500$ Hz which is the predefined frequency of the first subglottal resonance. This can be understood in terms of the supraglottal behaviour shown in Fig. 7 since both the VT and the SGT resonators have been realised similarly within the full model. The sensitivity of the f_0 trajectory in the range [180 Hz, 360 Hz] for the subglottal effect depends on the magnitude of the SGT component of the counter pressure, regulated by the parameter c_3 in Eq. (12). Considering the model behaviour at supraglottal subresonances of $\tilde{R}_1[q]$ as explained in Section 7, it is to be expected that the first subglottal subharmonic $\tilde{R}_1/2$ should show up similarly. This, indeed, happens if the coupling constant c_3 is large; see the discussion in Section 4.3.

8.3 Flow model

The glottal flow described by Eqs. (5)–(6) contains terms representing both the viscous and turbulent pressure loss in glottis. Viscous pressure loss can easily be seen to be significant by considering the glottal dimensions and viscosity of air in the first term of Eq. (6). It is clear from this equation that the viscous losses dominate at least if the glottal opening is small.

The importance of turbulence loss during parts of the glottal open phase can be seen, for example, by comparing simulated volume velocities and glottal opening areas with the experimental curves in [43, Fig. 3 on p. 628], obtained from a physical model of glottis. In model simulations, leaving out the turbulence term changes the glottal pulse waveform significantly if other model parameters are kept the same as shown in [28, Fig. 3.7]. About half of the total pressure loss in simulations is due to turbulence at the peak of opening

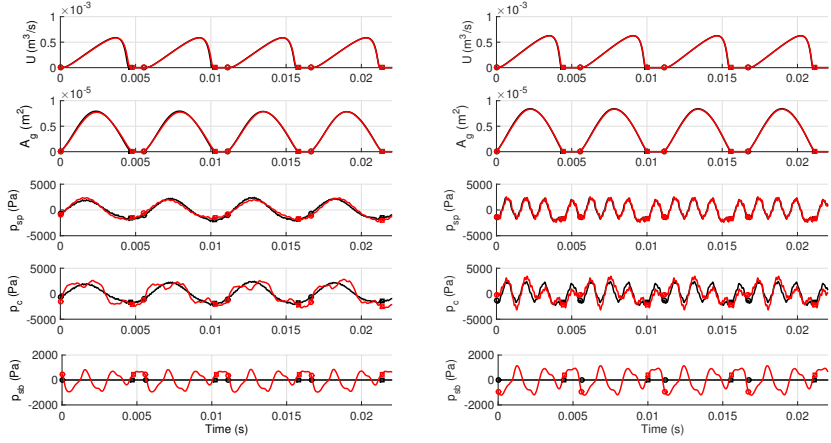


Figure 7: Left: Volume flow (U), glottal area (A_g), supraglottal pressure (p_{sp}) just superior to the vocal folds, counter pressure (p_c), and subglottal pressure just inferior to the vocal folds (p_{sb}) without SGT (black line) and with SGT (red line) for the vowel [i] at $f_0 = 180$ Hz. Glottal closure are indicated by squares and openings by circles. Right: Similar signals for the vowel [a].

of the glottis; see [28, Fig. 3.6]. However, the behaviour of the simulated f_0 trajectories over $R_1[i]$ does not change if the turbulence loss term is removed. Then, however, the vowel glide must be produced by different model parameter values.

9 Discussion

We have reported consistent observations on the locking of simulated f_0 glides on a resonance of the VT. The locking behaviour shows a consistent time-dependent behaviour that is similar for rising and falling glides. The locking takes place only at frequencies determined by sub- or supraglottal resonances. By modifying the strength of the acoustic feedback (i.e., the parameter Q_{pc} in Eq. (12)) and vocal fold tissue losses (i.e., the parameter β), the locking tendency at $R_1[i]$ may be modulated from non-existent (where both Q_{pc} and β have low values) to extreme locking at $R_1[i]$ without release (where Q_{pc} and/or β have exaggeratedly large values); see Fig. 6. By decoupling secondary components from the simulation model as explained in Section 8 above, the locking behaviour at $R_1[i]$ remains the same, even though the model parameter values required for the desired glottal pulse change. We conclude that the results reported in Section 7 reflect the *model behaviour* in a consistent and a robust manner.

Vowel glides observed in test subjects are another matter. Any model is a simplification of reality, and there is a catch in assessing the role of unmodelled physics: a proper treatment would require the modelling of it. Short of this, we discuss these aspects based on literature, model experiments, and reasoning by analogy.

Acoustics

Viscosity of air has not been taken into account in the acoustics model though a measurable effect is likely to take place in narrow parts of the VT or SGT. Resulting attenuation can be treated by adding a dissipation term of Kelvin–Voigt type to Eqs. (8) and (11). For a constant diameter waveguide, the term is proportional to $\mu\psi_{sst}/c^2$. Adding viscosity losses will widen and lower the resonance peaks of Webster’s resonators (i.e., lower their Q-value), with a slight change in the centre frequencies. An analogous effect can be studied by increasing the tissue dissipation parameter α in Eq. (8) to a very high value which has been observed not to change the conclusions of Section 7.

The SGT modelling by the horn is a crude simplification of the fractal-like lower airways and lungs. The network structure of the subglottal model in [27] could be replicated by interconnecting a large number of Webster’s resonators, each modelled by Eq. (11). The resulting *transmission graph* is a passive dynamical system by [66, Section 5], but it is not clear how to write an efficient FEM solver for such configurations.

The model proposed in [27] as well as the transmission graph approach are likely to produce the correct resonance distribution and frequency-dependent energy dissipation rate at the lung end without tuning. The horn model does require tuning of the horn opening area and the boundary condition on it in order to get realistic behaviour on the lowest subglottal resonance $\tilde{R}_1 = 500$ Hz. Doing so freezes all the higher subglottal resonances at fixed positions, e.g., $\tilde{R}_2 = 1.230$ kHz. The branching subglottal models given in [27, Fig. 8] have the second subglottal resonance between 1.3kHz and 1.5kHz.

Based on the observations of Section 7, it seems likely that the overall subglottal effect on the fundamental frequency f_0 is insignificant for vowel glides within [180 Hz, 360 Hz] that is over 100 Hz away from \tilde{R}_1 . However, the subglottal effect is certainly discernible in waveforms as in Fig. 7, but the effect of higher subglottal formants $\tilde{R}_2, \tilde{R}_3, \dots$ cannot be seen even there. In current simulations of female phonation, the vocal fold mass-spring system has its mechanical resonances at approximately 150 Hz, which acts as a low-pass filter for subglottal excitation in higher frequencies. The same conclusions are likely to hold when using a more complicated subglottal resonator geometry with one caveat: a graph-like subglottal geometry has lots of cross-mode resonances that affect the subglottal acoustic impedance in other ways than just moving the pole positions.

Vocal fold geometry and glottal flow

The idealised vocal folds geometry shown in Fig. 1 leads to a particularly simple expression for the aerodynamic force in Eq. (7). Replacing the sharp peaks by flat tops in Fig. 1 (but keeping the same glottal gap g at rest) results in phonation that has typically lower open quotient (OQ) whereas the original wedge-like geometry produces more often phonation where the glottis does not close. However, these changes do not affect the conclusions of Section 7.

The glottal flow has been studied extensively since 1950’s. Compared to the model given in Section 3, physiologically more faithful glottal flow solvers have been proposed in, e.g., Pelorson et al. (1994) in [35], Titze (2002) in [67], and Erath et al. (2011) in [68]; see also [49, 10, 69, 43, 26]. As pointed out in

[69, p. 83], more sophisticated flow models are challenging to couple to acoustic resonators since the interface between the flow-mechanical (in particular, the turbulent) and the acoustic components is no longer clearly defined. We next discuss improvements of glottal flow modelling in terms of including *flow separation* and *turbulence as an acoustic source*.

Flow separation and Coandă effect during the diverging phase of the phonatory cycle (which obviously cannot occur in wedge-like geometry of Fig. 1) have been studied in [68, 70, 35] using boundary layer theory and physical model experiments. The boundary layer leaves the vocal fold surfaces at the time-dependent flow separation point, say x_s , forming a jet which extends downstream into supraglottal space. Thus, the vocal folds “stall” at x_s , and the aerodynamic force on them is greatly diminished; see [68, Section. IV] where the vocal folds model is from [71]. Similarly, the viscous pressure loss in [35, Eq. (A7)] depends only on the upstream part of glottis that ends at x_s . Simplifying assumptions on the vocal fold geometry [35, Fig. 13] are required for computing x_s , and the result is sensitive to the geometry which makes it challenging to model.

Turbulence in supraglottal space is a spatially distributed acoustic source, and it does not provide a scalar flow velocity signal for boundary control as v_0 in Eq. (10). The supraglottal jet may even exert an additional aerodynamic force to vocal folds that would not be part of the acoustic counter pressure p_c from the acoustic resonators. Turbulence in VT constrictions is the primary acoustic source for unvoiced fricatives, and many such sources have been modelled separately in, e.g., [49]. Much of the turbulence noise energy lies above 4 kHz but Webster’s model Eq. (8) is an accurate description of VT acoustics only below 4 kHz due to the lack of cross-modes [60, 72, 73]. This fact speaks against the wisdom of including turbulence noise in the proposed model.

The model given in Sections 2–4 treats flow-mechanical and acoustic components using separate equations, and we conclude that this paradigm is not conducive for including the advanced flow-mechanical features discussed above. Instead, phonation models based on Navier–Stokes equations would be a more appropriate framework.

10 Conclusions

We have presented a model for vowel production, based on (partial) differential equations, that consists of submodels for glottal flow, vocal folds oscillations, and acoustic responses of the VT and subglottal cavities. The model has been originally designed as a tunable glottal pulse source for a high-resolution VT acoustics simulator that is based on the 3D wave equation and VT geometries obtained by MRI as explained in [4, 5, 50]. The model has found applications as a controlled source of synthetic vowels that are needed in, e.g., developing speech processing algorithms such as the inverse filtering [7, 8].

In this article, the model was used for simulations of rising and falling vowel glides of [a, i] in frequencies that span one octave [180 Hz, 360 Hz]. This interval contains the lowest VT resonance R_1 of [i] but not that of [a]. Perturbation events in simulated vowel glides were observed at VT acoustic resonances, or at some of their fractions (i.e., subresonances) but nowhere else. The fundamental frequency f_0 of the simulated vowel was observed to lock to $R_1[i]$ but similar

locking was not seen at any of the subresonances. Such modal locking event takes place only when the acoustic feedback from VT to vocal folds is present, and then it has a characteristic time-dependent behaviour. A large number of simulation experiments were carried out with different parameter settings of the model to verify the robustness and consistency of all observations.

To what extent do the simulation results validate the proposed model? The model produces perturbations of the glottal pulse both at VT resonances and at some of the VT subresonances. Of the former, a wide literature exists as reviewed in Section 1. Observations on the subresonance perturbations in speech have not been reported, to our knowledge, in experimental literature. There is a particular temporal pattern of locking in simulated perturbations at R_1 [i] as explained in Fig. 6 (left panel). Such a pattern can be seen in the speech spectrograms given in [17, Fig. 5], [16, Fig. 4], and in vowel glide samples in the data set of the companion article [3]. The glottal flow and area simulations in Fig. 7 are remarkably similar with the experimental data presented in [52, Figs. 4-7], the signals produced by different numerical models [10, Figs. 14a-14c], [40, Figs. 8 and 10], [27, Figs. 10-11], [67, Fig. 6], [74, Fig. 5], and the glottal pulse waveforms obtained by inverse filtering in, e.g., [8, Figs. 10-13], [75, Figs. 5.3, 5.4, and 5.17], [42], and [7, Figs. 3 and 6].

In simulations, we have disregarded the neural control actions to the vocal fold structures and modifications of the VT geometry. There is also a significant control action affecting the subglottal pressure and it has been used as a control variable in Eqs. (15)–(16) for glide productions. In humans, neural control actions are part of feedback loops, of which some are auditive, and some others operate directly through tissue innervation and the central nervous system. So little is known about these feedback mechanisms that their explicit mathematical modelling seems hopeless. Instead, the model parameters for simulations are tuned so that the simulated glottal pulse waveform corresponds to experimental speech data.

Neglecting the role of neural control actions, we conjecture that the leading source of discrepancy between the model and true speech biophysics in vowels is due to simplified flow modelling for frequencies under 4 kHz. For frequencies over 4 kHz, modelling VT acoustics by Webster’s equation (as opposed to the 3D wave equation) is insufficient.

Acknowledgements

The authors were supported by the Finnish graduate school in engineering mechanics, Finnish Academy project Lastu 135005, 128204, and 125940; European Union grant Simple4All (grant no. 287678), Aalto Starting Grant 915587, and Åbo Akademi Institute of Mathematics. The authors would like to thank two anonymous reviewers for comments leading to improvements of the model.

References

- [1] T. Chiba, M. Kajiyama, *The Vowel, its Nature and Structure*, Tokyo-Kaiseikan, 1941.
- [2] G. Fant, *The Acoustic Theory of Speech Production*, Moulton, The Hague, 1960.

- [3] A. Aalto, D. Aalto, J. Malinen, M. Vainio, Modal locking between vocal fold and vocal tract oscillations: Experiments and statistical analysis, arXiv:1211.4788. (2013).
- [4] D. Aalto, O. Aaltonen, R.-P. Happonen, P. Jääsaari, A. Kivelä, J. Kuortti, J. M. Luukinen, J. Malinen, T. Murtola, R. Parkkola, J. Saunavaara, M. Vainio, Large scale data acquisition of simultaneous MRI and speech, *Appl Acoust* 83 (1) (2014) 64–75.
- [5] D. Aalto, O. Aaltonen, R.-P. Happonen, J. Malinen, P. Palo, R. Parkkola, J. Saunavaara, M. Vainio, Recording speech sound and articulation in MRI, in: *Proceedings of BIODEVICES 2011*, Rome, 2011, pp. 168–173.
- [6] P. Alku, J. Pohjalainen, M. Vainio, A.-M. Laukkanen, B. Story, Formant frequency estimation of high-pitched vowels using weighted linear prediction, *J. Acoust. Soc. Am.* 134 (2) (2013) 1295–1313.
- [7] P. Alku, Glottal inverse filtering analysis of human voice production - A review of estimation and parameterization methods of the glottal excitation and their applications, *Sadhana, Springer-Verlag* 36 (2011) 623–650
- [8] P. Alku, Glottal wave analysis with pitch synchronous iterative adaptive inverse filtering, *Speech Commun* 11 (2–3) (1992) 109–118.
- [9] B. Story, Speech simulation with an enhanced wave-reflection model of the vocal tract, Doctoral dissertation, University of Iowa, Iowa City (1994).
- [10] K. Ishizaka, J. Flanagan, Synthesis of voiced sounds from a two mass model of the vocal cords, *Bell System Technical Journal* 51 (1972) 1233–1268.
- [11] S. Austin, I. Titze, The effect of subglottal resonance upon vocal fold vibration, *J Voice* 11 (4) (1996) 391–402.
- [12] Z. Zhang, J. Neubauer, D. Berry, The influence of subglottal acoustics on laboratory models of phonation, *J. Acoust. Soc. Am.* 120 (3) (2005) 1558–1569.
- [13] J. Lucero, K. Lourenço, N. Hermant, A. Van Hirtum, X. Pelorson, Effect of source-tract acoustical coupling on the oscillation onset of the vocal folds, *J. Acoust. Soc. Am.* 132 (1) (2012) 403–411.
- [14] I. Titze, Nonlinear source-filter coupling in phonation: Theory, *J. Acoust. Soc. Am.* 123 (5) (2008) 2733–2749.
- [15] H. Hatzikirou, W. Fitch, H. Herzel, Voice instabilities due to source-tract interactions, *Acta Acustica united with Acustica* 92 (2006) 468–475.
- [16] I. Tokuda, M. Zemke, M. Kob, H. Herzel, Biomechanical modeling of register transitions and the role of vocal tract resonators, *J. Acoust. Soc. Am.* 127 (3) (2010) 1528–1536.
- [17] I. Titze, T. Riede, P. Popolo, Nonlinear source-filter coupling in phonation: Vocal exercises, *J. Acoust. Soc. Am.* 123 (4) (2008) 1902–1915.

- [18] M. Zañartu, D. D. Mehta, J. C. Ho, G. R. Wodicka, R. E. Hillman, Observation and analysis of *in vivo* vocal fold tissue instabilities produced by nonlinear source-filter coupling: A case study, *J. Acoust. Soc. Am.* 129 (1) (2011) 326–339.
- [19] K. Kelly, C. Lochbaum, Speech synthesis, in: Proceedings of the Fourth International Congress on Acoustics, Paper G42, 1962, pp. 1–4.
- [20] H. K. Dunn, The calculation of vowel resonances, and an electrical vocal tract, *J. Acoust. Soc. Am.* 22 (1950) 740 – 753.
- [21] S. El Masri, X. Pelorson, P. Saguet, P. Badin, Development of the transmission line matrix method in acoustics. Applications to higher modes in the vocal tract and other complex ducts, *Int. J. Numerical Modelling* 11 (1998) 133 – 151.
- [22] J. Mullen, D. Howard, D. Murphy, Waveguide physical modeling of vocal tract acoustics: Flexible formant bandwidth control from increased model dimensionality, *IEEE Trans. Audio, Speech, Language Process.* 14 (3) (2006) 964 – 971.
- [23] S. Rienstra, A. Hirschberg, An introduction to acoustics, 2013. <http://www.win.tue.nl/~sjoerdr/papers/boek.pdf>.
- [24] K. van den Koel, U. Ascher, Real-time numerical solution of Webster's equation on a nonuniform grid, *IEEE Trans. Audio, Speech, Language Process.* 16 (6) (2008) 1163–1172.
- [25] J. Horáček, V. Uruba, V. Radolf, J. Veselý, V. Bula, Airflow visualization in a model of human glottis near the self-oscillating vocal folds model, *Applied and Computational Mechanics* 5 (2011) 21–28.
- [26] P. Šidlof, J. Horáček, V. Řídký, Parallel CFD simulation of flow in a 3D model of vibrating human vocal folds, *Computers & Fluids* 80 (2013) 290–300.
- [27] H. Ho, M. Zañartu, G. Wodicka, An anatomically based, time-domain acoustic model of the subglottal system for speech production, *J. Acoust. Soc. Am.* 129 (3) (2011) 1531–1547.
- [28] T. Murtola, Modelling vowel production, Licentiate thesis, Aalto University School of Science (2014).
- [29] H. Gray, *Anatomy of the Human Body*, Lea & Febiger, Philadelphia, 1918.
- [30] A. Aalto, A low-order glottis model with nonturbulent flow and mechanically coupled acoustic load, Master's thesis, Helsinki University of Technology, Institute of Mathematics (2009).
- [31] A. Aalto, D. Aalto, J. Malinen, M. Vainio, Interaction of vocal fold and vocal tract oscillations, in: Proceedings of the 24th Nordic Seminar on Computational Mechanics, 2011.

- [32] J. Horáček, P. Šídlof, J. Švec, Numerical simulation of self-oscillations of human vocal folds with Hertz model of impact forces, *J Fluid Struct* 20 (2005) 853–869.
- [33] J. Liljencrants, A translating and rotating mass model of the vocal folds, *STL-QPSR* 32 (1) (1991) 1–18.
- [34] N. Lous, G. Hofmans, R. Veldhuis, A. Hirschberg, A symmetrical two-mass vocal-fold model coupled to vocal tract and trachea, with application to prosthesis design, *Acta Acustica united with Acustica* 84 (6) (1998) 1135–1150.
- [35] X. Pelorson, A. Hirschberg, R. van Hassel, A. Wijnands, Theoretical and experimental study of quasisteady-flow separation within the glottis during phonation. Application to a modified two-mass model, *J. Acoust. Soc. Am.* 96 (6) (1994) 3416–3431.
- [36] B. Story, I. Titze, Voice simulation with a body-cover model of the vocal folds, *J. Acoust. Soc. Am.* 97 (2) (1995) 1249–1260.
- [37] P. Birkholz, A survey of self-oscillating lumped-element models of the vocal folds, *Studientexte zur Sprachkommunikation: Elektronische Sprachsignalverarbeitung* (2011) 47–58.
- [38] B. Erath, M. Zañartu, K. Stewart, M. Plesniak, D. Sommer, S. D. Peterson, A review of lumped-element models of voiced speech, *Speech Commun* 55 (5) (2013) 667 – 690.
- [39] F. Alipour, C. Brücker, D. Cook, A. Gömmel, M. Kaltenbacher, W. Mattheus, L. Mongeau, E. Nauman, R. Schwarze, I. Tokuda, S. Zörner, Mathematical models and numerical schemes for the simulation of human phonation, *Current Bioinformatics* 6 (2011) 323–343.
- [40] M. Zañartu, L. Mongeau, G. Wodicka, Influence of acoustic loading on an effective single mass model of the vocal folds, *J. Acoust. Soc. Am.* 121 (2007) 1119–1129.
- [41] J. Horáček, J. Švec, Aeroelastic model of vocal-fold-shaped vibrating element for studying the phonation threshold, *J Fluid Struct* 16 (7) (2002) 931–955.
- [42] A. Aalto, P. Alku, J. Malinen, A LF-pulse from a simple glottal flow model, in: *Proceedings of the 6th International Workshop on Models and Analysis of Vocal Emissions for Biomedical Applications (MAVEBA2009)*, Firenze, 2009, pp. 199–202.
- [43] J. van den Berg, J. Zantema, P. Doornenbal, On the air resistance and the Bernoulli effect of the human larynx, *J. Acoust. Soc. Am.* 29 (5) (1957) 626–631.
- [44] L. Fulcher, R. Scherer, T. Powell, Pressure distributions in a static physical model of the uniform glottis: Entrance and exit coefficients, *J. Acoust. Soc. Am.* 129 (3) (2011) 1548–1553.

- [45] T. Lukkari, J. Malinen, Webster's equation with curvature and dissipation, arXiv:1204.4075, submitted, (2013).
- [46] A. Aalto, T. Lukkari, J. Malinen, Acoustic wave guides as infinite-dimensional dynamical systems, *ESAIM Contr Optim Ca* 21 (2) (2015) 324–347.
- [47] T. Lukkari, J. Malinen, A posteriori error estimates for Webster's equation in wave propagation, *J Math Anal Appl* 427 (2) (2015) 941–961.
- [48] P. Morse, K. Ingard, *Theoretical Acoustics*, McGraw–Hill, 1968.
- [49] P. Birkholtz, D. J. el, B. Kröger, Simulation of losses due to turbulence in the time-varying vocal system, *IEEE Trans. Audio, Speech, Language Process.* 15 (4) (2007) 1218–1226.
- [50] D. Aalto, J. Helle, A. Huhtala, A. Kivelä, J. Malinen, J. Saunavaara, T. Ronkka, Algorithmic surface extraction from MRI data: modelling the human vocal tract, in: *Proceedings of BIOVICES 2013*, 2013, pp. 257–260.
- [51] A. Kivelä, *Acoustics of the vocal tract: MR image segmentation for modelling*, Master's thesis, Aalto University School of Science (2015).
- [52] B. Cranen, L. Boves, Pressure measurements during speech production using semiconductor miniature pressure transducers: Impact on models for speech production, *J. Acoust. Soc. Am.* 77 (4) (1985) 1543–1551.
- [53] B. Cranen, L. Boves, On subglottal formant analysis, *J. Acoust. Soc. Am.* 81 (3) (1987) 734–746.
- [54] I. Titze, Physiologic and acoustic differences between male and female voices, *J. Acoust. Soc. Am.* 85 (4) (1989) 1699–1707.
- [55] D. Chhetri, Z. Zhang, J. Neubauer, Measurement of Young's modulus of vocal folds by indentation, *J Voice* 25 (2011) 1–7.
- [56] D. Scimarella, C. d'Alessandro, On the acoustic sensitivity of a symmetric two-mass model of the vocal folds to the variation of control parameters, *Acta Acoustica united with Acustica* 90 (2004) 746–761.
- [57] P. Lieberman, R. Knudson, J. Mead, Determination of the rate of change of fundamental frequency with respect to subglottal air pressure during sustained phonation, *J. Acoust. Soc. Am.* 45 (6) (1969) 1537–1543.
- [58] I. Titze, On the relation between subglottal pressure and fundamental frequency in phonation, *J. Acoust. Soc. Am.* 85 (2) (1989) 901–906.
- [59] V. Havu, J. Malinen, Cayley transform as a time discretization scheme, *Numer Func Anal Opt.* 28 (7) (2007) 825–851.
- [60] A. Kivelä, J. Kuortti, J. Malinen, Resonances and mode shapes of the human vocal tract during vowel production, in: *Proceedings of 26th Nordic Seminar on Computational Mechanics*, 2013, pp. 112–115.

- [61] K. Neumann, V. Gall, H. Schutte, D. Miller, A new method to record subglottal pressure waves: potential applications, *J Voice* 17 (2) (2003) 140–159.
- [62] Y. Koike, M. Hirano, Glottal-area time function and subglottal-pressure variation, *J. Acoust. Soc. Am.* 54 (6) (1973) 1618–1627.
- [63] E. Weibel, *Morphometry of the Human Lung*, Springer, Berlin, 1963.
- [64] H. Yeh, G. Schum, Models of human-lung airways and their application to inhaled particle deposition, *Bull. Math. Biol.* 42 (1980) 461–480.
- [65] D. Sciamarella, G. Artana, A water hammer analysis of pressure and flow in the voice production system, *Speech Commun* 51 (2009) 344–351.
- [66] A. Aalto, J. Malinen, Composition of passive boundary control systems, *Math Control Relat F* 3 (1) (2013) 1–19.
- [67] I. Titze, Regulating glottal airflow in phonation: Application of the maximum power transfer theorem to a low dimensional phonation model, *J. Acoust. Soc. Am.* 111 (1) (2002) 367–376.
- [68] B. Erath, S. Peterson, M. Zaňartu, G. Wodicka, M. Plesniak, A theoretical model of the pressure field arising from asymmetric intraglottal flows applied to a two-mass model of the vocal folds, *J. Acoust. Soc. Am.* 130 (1) (2011) 389–403.
- [69] P. Punčochářová-Pořízková, K. Kozel, J. Horáček, J. Fürst, Numerical simulation of unsteady compressible low mach number flow in a channel, *Engineering Mechanics* 17 (2–3) (2010) 83–97.
- [70] B. Erath, M. Plesniak, An investigation of asymmetric flow features in a scaled-up model of the human vocal folds, *Exp. Fluids* 49 (2010) 131–146.
- [71] I. Steinecke, H. Herz, Bifurcations in an asymmetric vocal-fold model, *J. Acoust. Soc. Am.* 97 (1995) 1874–1884.
- [72] T. Vampola, J. Horáček, A.-M. Laukkanen, J. Švec, Finite element modelling of vocal tract changes after voice therapy, *Applied and Computational Mechanics* 5 (1) (2011) 77–88.
- [73] T. Vampola, J. Horáček, A.-M. Laukkanen, J. Švec, Human vocal tract resonances and the corresponding mode shapes investigated by three-dimensional finite-element modelling based on CT measurement, *Logopedia Phoniatrics Vocology* (2013) 1–10.
- [74] I. Titze, Parameterization of the glottal area, glottal flow, and vocal fold contact area, *J. Acoust. Soc. Am.* 75 (2) (1984) 570–580.
- [75] H. Pulakka, Analysis of human voice production using inverse filtering, high-speed imaging, and electroglottography, Master's thesis, Helsinki University of Technology, Department of Computer Science and Engineering (2005).